Available online at www.sciencedirect.com
SCIENCE DIRECT®
International Journal of Heat and Mass Transfer 48 (2005) 3628–3636
International Journal of HEAT and MASS TRANSFER
www.elsevier.com/locate/ijhmt

The creeping flow of a polymeric fluid through bent square ducts with heat dissipation

G.H. Wu *

Department of Mechanical Engineering, National Cheng-Kung University, Tainan 701, Taiwan, ROC

Received 12 January 2004; received in revised form 11 November 2004
Available online 2 June 2005

Abstract

The 3D non-isothermal creeping flow of nylon-6 in a bent square duct with uniform temperature is studied numerically. The non-Newtonian characteristics of this fluid polymer are represented by a differential-type non-isothermal White–Metzner model. Computational results are obtained by the elastic-viscous split-stress (EVSS) finite element method, incorporating the streamline-upwind Petrov–Galerkin (SUPG) scheme. The generated thermal field is entirely due to viscous heating. Essential flow characteristics, including temperature distribution in the flow field, are predicted. The resulting average Nusselt numbers along the walls are obtained. Subsequently, the effects of flow-rate and geometry are investigated.

Keywords: Viscous heating; Finite element method; Rectangular duct; Nusselt number

1. Introduction

Flow of a polymeric or viscoelastic fluid in a bent square duct is of significant importance in polymer processing. The study of such flows is thus of some significance and has attracted a great deal of attention in the literature.

There have been a number of studies on the case of laminar flows of non-Newtonian (inelastic) fluids in ducts. Hwang and Hong [1] analytically and experimentally investigated the influence of variable viscosity on the laminar heat transfer in a square duct for the constant wall temperature condition with ethylene glycol. They reported that the Nusselt numbers increased by approximately 15–20% from the values of constant property fluid. Ahmadian et al. [2] numerically studied the 3D laminar flow with and without partial solidification of an initial molten polymer in square ducts with a 90° curve. The non-Newtonian characteristics of the fluid polymer were represented by a differential-type non-isothermal power-law model. The result of a larger heat transfer coefficient at the outer boundary than at the inner boundary was presented.

Turning to viscoelastic fluids, several researchers conducted experimental studies on the flow through rectangular ducts under laminar conditions. In 1971, Oliver and Rao [3] experimentally found that viscoelastic fluids in laminar flow through flattened tubes gave higher heat transfer coefficients than Newtonian fluids of the same Prandtl number. Mena et al. [4] also reported higher heat transfer coefficients for a viscoelastic fluid in laminar flow through rectangular ducts as compared to the corresponding Newtonain fluid. He concluded that the

* Tel.: +886 6 2757575x62179; fax: +886 6 2208643.
E-mail address: d1014519@mail.ncku.edu.tw

0017-9310/$ - see front matter © 2005 Elsevier Ltd. All rights reserved.
doi:10.1016/j.ijheatmasstransfer.2004.11.025

Nomenclature

A	cross-sectional area, m^2
C_p	heat capacity, kJ/kg °C
D_e	Dean number
D_h	hydraulic diameter, m
$\boldsymbol{d}$	rate-of-deformation tensor, s^{-1}
N_1	the primary normal-stress difference, N/m^2
N_u	local Nusselt number
$\overline{N}_u$	average Nusselt number of each wall at a specified streamline location
p	pressure, N/m^2
P_e	Peclet number
R	corner radius, m
R_e	Reynolds number
S^*	dimensionless streamline coordinate
$\boldsymbol{s}$	the elastic part of the viscoelastic stress $\boldsymbol{\tau}$, N/m^2
T_b^*	dimensionless bulk-mean temperature
v_s	the velocity along the streamline, m/s
W_e	Weissenberg number
$\boldsymbol{U}$	mean inlet velocity, m/s
Greek symbols	
∇	gradient operator, m^{-1}
ρ	density, kg/m^3
$\boldsymbol{\tau}$	the viscoelastic stress of the polymer liquid, N/m^2
$\boldsymbol{\tau}_{(1)}$	the upper convected derivative of the viscoelastic stress $\boldsymbol{\tau}$, $N/(m^2\,s)$
$\boldsymbol{d}_{(1)}$	the upper-convected derivative of the strain-rate tensor, s^{-2}
$\dot{\boldsymbol{\gamma}}$	shear-rate tensor, s^{-1}
$\dot{\gamma}$	shear-rate, s^{-1}
$\dot{\gamma}_c$	characteristic shear-rate, s^{-1}
λ	relaxation-time, s
ϕ_i	quadratic basic function
ψ_i	bilinear basic function

laminar flow of viscoelastic fluids through non-circular rectangular geometries is accompanied by secondary flows caused by elastic effects which have significant effects on the heat-transfer enhancement. Hartnett and Kostic [5] measured the local Nusselt numbers for aqueous polycrylamide solutions, viscoelastic fluids, in laminar flow through a rectangular channel. The measured values were found to be much higher than those of a purely viscous fluid. They concluded that the heat transfer enhancement might be due to the secondary flows arising from elastic effect. Xie and Hartnett [6] did experimental studies on the heat-transfer behavior for two types of aqueous polymer solutions in a rectangular channel. The measured Nusselt values for the two polymer solutions were considerably higher than the values for a corresponding in-elastic power-law fluid and higher than the experimental values for water.

The creeping flow of 3D non-isothermal viscoelastic fluid in bent square ducts has not yet been studied numerically. The objective of the present study is to investigate the creeping heat-transfer behavior of this type of flow numerically for a nylon-6 liquid using the EVSS/SUPG finite element method. The mathematical model used for this flow simulation is a differential-type non-isothermal White–Metzner constitutive equation, which describes the non-Newtonian behavior of nylon-6. Since the Dean number [7], defined as $D_e = R_e(D_h/R)^{0.5}$, is small for this type of flow, centrifugal force is neglected in the momentum equation. Essential flow characteristics, including temperature distribution in the flow field, are predicted. The resulting average Nusselt numbers along the walls are obtained. Subsequently, the effects of flow-rate and geometry are investigated.

2. Mathematical modelling

Fig. 1 illustrates the flow geometry of the present problem. The dimensions used are as follows: $l = 0.015$ m, $w = 0.002$ m, $h = 0.002$ m, and $R_i = 0.004$ m. The aspect ratio h/w is equal to 1. It is well known that non-isothermal flow of a viscoelastic fluid is governed by the following set of conservation and constitutive equations.

Continuity equation:

$$\nabla \cdot \upsilon = 0 \tag{1}$$

Momentum equation, neglecting body forces:

$$\rho(\upsilon \cdot \nabla)\upsilon = -\nabla p + \nabla \cdot \boldsymbol{\tau} \tag{2}$$

where $\boldsymbol{\tau}$ is the extra stress.

The total stress tensor is expressed as

$$\boldsymbol{\sigma} = -p\boldsymbol{I} + \boldsymbol{\tau} \tag{3}$$

where p is pressure and $\boldsymbol{I}$ is the unit tensor.

For fluids with constant density ρ, heat capacity C_p, and thermal conductivity k, the energy equation is given as

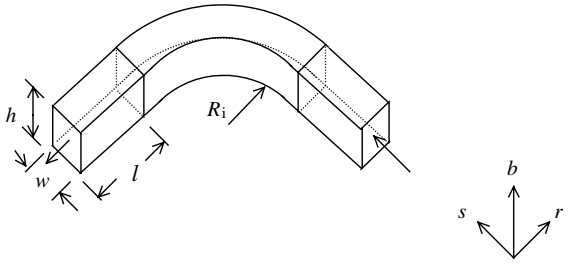

Fig. 1. Flow geometry.

Table 1
Rheological data and material functions used in the non-isothermal White–Metzner model for nylon-6

$\eta = \eta(\dot{\gamma}, T) = \eta_0(T)[1 + (\lambda_1\dot{\gamma})^2]^{(n-1)/2}$	$\rho = 986\ \text{kg m}^{-3}$
$\eta_0(T) = \eta_{0,\text{ref}} \exp[\beta_1(1/T - 1/T_{\text{ref}})]$	$C_p = 1450\ \text{J kg}^{-1}\ \text{K}^{-1}$
$\lambda_0(T) = \lambda_{1,\text{ref}} \exp[\beta_2(1/T - 1/T_{\text{ref}})]$	$k = 0.25\ \text{W m}^{-1}\ \text{K}^{-1}$
$\eta_0(T_w) = \eta_{0,\text{ref}} = 368.7\ \text{N s m}^{-2}$	$n = 0.7678$
$\psi_1(\dot{\gamma}, T) = \psi_{1,0}(T)[1 + (\lambda_2\dot{\gamma})^2]^{(n'-2)/2}$	$\beta_1 = 8327\ \text{K}$
$\psi_{1,0}(T) = \psi_{1,0,\text{ref}} \exp[\beta_3(1/T - 1/T_{\text{ref}})]$	$\beta_2 = 17\,300\ \text{K}$
$\lambda_2(T) = \lambda_{2,\text{ref}} \exp[\beta_4(1/T - 1/T_{\text{ref}})]$	$\beta_3 = 18\,630\ \text{K}$
$\psi_{1,0}(T_w) = \psi_{1,0,\text{ref}} = 12.66\ \text{N s}^2\ \text{m}^{-2}$	$\beta_4 = 5113\ \text{K}$
$\lambda_{1,\text{ref}} = 0.01766\ \text{s}$	$n' = 1.2$
$\lambda_{2,\text{ref}} = 0.1455\ \text{s}$	$T_w = 535\ \text{K}$
$T_{\text{ref}} = 535\ \text{K}$	

$$\rho C_p \upsilon \cdot \nabla T = \nabla \cdot k(\nabla T) + \boldsymbol{\tau} : \boldsymbol{d} \tag{4}$$

where $\boldsymbol{d} = (\nabla\upsilon + \nabla\upsilon^{\text{T}})/2$.

The non-isothermal White–Metzner equation used by Finlayson [8] to model the non-isothermal flow of nylon-6 is defined by the following equation, together with the curve-fitted parameters and material functions in Table 1.

$$\boldsymbol{\tau} + \lambda\boldsymbol{\tau}_{(1)} = \eta\dot{\boldsymbol{\gamma}} \tag{5}$$

The meaning of each term in Eq. (5) are summarized as follows:

Upper convective derivative of the extra stress:

$$\boldsymbol{\tau}_{(1)} = \upsilon \cdot \nabla\boldsymbol{\tau} - \nabla\upsilon^{\text{T}} \cdot \boldsymbol{\tau} - \boldsymbol{\tau} \cdot \nabla\upsilon \tag{6}$$

Viscosity function $\eta = \eta(\dot{\gamma}, T)$.

Relaxation-time function: $\lambda = \lambda(\dot{\gamma}, T)$.

The relaxation-time function can be obtained via the following equation:

$$\lambda(\dot{\gamma}, T) = \psi_1(\dot{\gamma}, T)/2\eta(\dot{\gamma}, T) \tag{7}$$

where $\psi_1(\dot{\gamma}, T)$ is the primary normal stress function. The material functions $\lambda(\dot{\gamma}, T)$, $\eta(\dot{\gamma}, T)$ and $\psi_1(\dot{\gamma}, T)$ are all temperature and shear-rate dependent. The shear-rate dependence is described by the Cross model, while the temperature dependence is of the Arrhenius type.

The velocity, stress and temperature profiles are considered to be fully developed at the inlet. For the outlet, the velocity is established by solving the problem using the corresponding in-elastic generalized Newtonian fluid model with zero normal-force and heat-flux imposed at the outlet. The wall temperature is constant throughout. *Outlet heat-flux is zero*. Also, no slip boundary condition is applied at the wall.

3. Numerical method

Recently, several finite element methods have been developed to overcome the convergence difficulties encountered when simulating 2D isothermal viscoelastic flow problems. Marchal and Crochet [9] applied the non-consistent/streamline-upwind method to discretize the constitutive equation for elastic-flow problems, and each element was subdivided into a 4×4 sub-element for stress analysis. This method showed good behavior for highly elastic 2D isothermal flow problems, but was expensive in terms of computer time. Another method, called the elastic-viscous split-stress (EVSS) finite element method, was proposed by Mendelson et al. [10] in 1983 to simulate the 2D isothermal flow of viscoelastic fluids with Newtonian viscosity such as the Oldroyd-B fluids. This method employs the splitting of the extra-stress into its viscous and elastic terms, and a change of variables for the momentum and the constitutive equations, yielding a set of equations involving the velocity υ, the pressure p, and the new elastic-stress $\boldsymbol{s}$. The rate-of-deformation tensor $\boldsymbol{d}$ is also introduced as an additional unknown, leading to a four-field $(\upsilon, p, \boldsymbol{s}, \boldsymbol{d})$ problem. In 1994, the EVSS finite element method incorporating the streamline-upwind/Petrov–Galerkin technique (known as the EVSS/SUPG finite element method) was proposed by Debae et al. [11] and proved to be accurate and stable for 2D isothermal viscoelastic flow problems with smooth boundaries. In 1999, Wu and Ju [12] simulated 2D non-isothermal viscoelastic flow of a nylon-6 liquid past a cylinder between plates, using EVSS/SUPG for a differential-type non-isothermal White–Metzner fluid. They reported that the drag on the cylinder decreases if temperature-thinning of the fluid is considered.

In the present study, the 2D EVSS/SUPG is extended to simulate the 3D non-isothermal creeping flow of White–Metzner fluids through bent square-ducts. In order to solve the present flow problem by this numerical method, the governing equations in EVSS form is first derived as follows.

3.1. Dimensionless governing equations in EVSS form

In the EVSS formulation, the viscoelastic stress is split into its elastic and viscous components:

$$\boldsymbol{\tau} = \boldsymbol{s} + 2\eta\boldsymbol{d}. \tag{8}$$

where $\boldsymbol{s}$ denotes the elastic component of the viscoelastic stress and $2\eta\boldsymbol{d}$ represents the viscous component.

Upon substituting $(\boldsymbol{s} + 2\eta\boldsymbol{d})$ for $\boldsymbol{\tau}$ into Eqs. (2)–(5), the governing equations in EVSS form become:

$$\nabla \cdot \upsilon = 0 \tag{9}$$

$$\upsilon \cdot \nabla\upsilon = \nabla \cdot (-p\boldsymbol{I} + \boldsymbol{s} + 2\eta\boldsymbol{d}) \tag{10}$$

$$\rho C_p \upsilon \cdot \nabla T = \nabla \cdot k(\nabla T) + (\boldsymbol{s} + 2\eta\boldsymbol{d}) : \boldsymbol{d} \tag{11}$$

$$\boldsymbol{s} + \lambda\left(\boldsymbol{s}_{(1)} + 2\eta\boldsymbol{d}_{(1)}\right) = 0 \tag{12}$$

$$\boldsymbol{d} - (\nabla\upsilon + \nabla\upsilon)^{\text{T}}/2 = 0 \tag{13}$$

When appropriate dimensionless variables are introduced, the dimensionless governing equations can be obtained as follows:

$$\nabla^* \cdot \upsilon^* = 0 \tag{14}$$

$$R_e \upsilon^* \cdot \nabla^* \upsilon^* = \nabla^* \cdot (-p^* \boldsymbol{I} + \boldsymbol{s}^* + 2\eta^* \boldsymbol{d}^*) \tag{15}$$

$$P_e \upsilon^* \cdot \nabla^* T^* = \nabla^{*2} T^* + \boldsymbol{B}_r (\boldsymbol{s}^* + 2\eta^* d^*) : \boldsymbol{d}^* \tag{16}$$

$$\boldsymbol{s}^* + W_e \lambda^* \left(\boldsymbol{s}^*_{(1)} + 2\eta^* \boldsymbol{d}^*_{(1)} \right) = 0 \tag{17}$$

$$\boldsymbol{d}^* - (\nabla^* \upsilon^* + \nabla^* \upsilon^{*\mathrm{T}})/2 = 0 \tag{18}$$

where the dimensionless variables are defined as: $\boldsymbol{x}^* = \boldsymbol{x}/w$, $\upsilon^* = \upsilon/U$, $\nabla^* = w\nabla$, $\eta^* = \eta/\eta_{0,\mathrm{ref}}$, $T^* = (T - T_\mathrm{w})/(T_\mathrm{b} - T_\mathrm{w})$, $p^* = pw/U\eta_{0,\mathrm{ref}}$, $d^* = w\boldsymbol{d}/U$, and $\boldsymbol{s}^* = \boldsymbol{s}w/U\eta_{0,\mathrm{ref}}$. T_b is conveniently defined as: $T_\mathrm{b} = T_\mathrm{w} + 1(K)$.

In these equations, the Reynolds number, Weissenberg number, Peclet number, and Brinkman are defined as:

$$R_e = \rho U w/\eta_{0,\mathrm{ref}} \tag{19}$$

$$W_e = U\lambda_{0,\mathrm{ref}}/w \tag{20}$$

$$P_e = \rho C_p w U/k \tag{21}$$

$$B_r = \eta_{0,\mathrm{ref}} U^2/k(T_\mathrm{b} - T_\mathrm{w}) \tag{22}$$

where $\eta_{0,\mathrm{ref}}$ and $\lambda_{0,\mathrm{ref}}$ are the viscosity and relaxation-time constant at zero- shear-rate and at reference temperature.

3.2. Weak formulation of the dimensionless governing equations

The dimensionless field variables are interpolated within each element by

$$\upsilon^* = \sum_{i=1}^{N=27} \phi_i \upsilon_i^* \quad p^* = \sum_{i=1}^{M=9} \psi_i p_i^*$$

$$\boldsymbol{s}^* = \sum_{i=1}^{M=9} \psi_i \boldsymbol{s}_i^* \quad \boldsymbol{d}^* = \sum_{i=1}^{M=9} \psi_i \boldsymbol{d}_i^*$$

$$T^* = \sum_{i=1}^{N=27} \phi_i T_i^*$$

where υ_i^*, p_i^*, $\boldsymbol{s}_i^*$, $\boldsymbol{d}_i^*$, T_i^* are nodal values and ϕ_i, ψ_i are tri-quadratic and tri-linear basic functions, respectively.

Following the traditional Galerkin's manipulations, the weak form of the dimensionless governing Eqs. (14), (15), and (18) can be derived as follows:

$$\int_\Omega \psi_i (\nabla^* \cdot \upsilon^*) \,\mathrm{d}\Omega = 0 \tag{23}$$

$$\int_\Omega [\phi_i (R_e \upsilon^* \cdot \nabla^* \upsilon^*) + \nabla^* \phi_i \cdot (-p^* \boldsymbol{I} + \boldsymbol{s}^* + 2\eta^* \boldsymbol{d}^*)] \,\mathrm{d}\Omega - \int_A \phi_i \boldsymbol{n} (-p^* \boldsymbol{I} + \boldsymbol{s}^* + 2\eta^* \boldsymbol{d}^*) \,\mathrm{d}A = 0 \tag{24}$$

$$\int_\Omega \psi_i [\boldsymbol{d}^* - (\nabla^* \upsilon^* + \nabla^* \upsilon^{*\mathrm{T}})/2] \,\mathrm{d}\Omega = 0 \tag{25}$$

The traditional Galerkin method is known to be inappropriate when the convective terms in the hyperbolic constitutive equations become dominant as the Weissenberg number increases. The streamline-upwind/Petrov–Galerkin (SUPG) technique proposed by Debae et al. is therefore applied to the constitutive equation (17). In this technique, an additional weighing function $(\bar{k}^* \upsilon^*/\upsilon^* \cdot \upsilon^*) \cdot \nabla^* \psi_i$ is applied to all the terms of the constitutive equation. The dimensionless $\bar{k}^*$ is proposed in this study as:

$$\bar{k}^* = [(\upsilon_\xi^* h_\xi^*)^2 + (\upsilon_\chi^* h_\chi^*)^2 + (\upsilon_\eta^* h_\eta^*)^2]/2 \tag{26}$$

in which the definition of dimensionless velocity components $(\upsilon_\xi^*, \upsilon_\chi^*, \upsilon_\eta^*)$ at the element center and element characteristic lengths $(h_\xi^*, h_\chi^*, h_\eta^*)$ are defined in [13]. Hence, the weak form of Eq. (17) is then obtained as

$$\int_\Omega [\psi_i + (\bar{k}^* \upsilon^*/\upsilon^* \cdot \upsilon^*) \cdot {}^*\psi_i] \times [\boldsymbol{s}^* + W_e \lambda^* (\boldsymbol{s}^*_{(1)} + 2\eta^* \boldsymbol{d}^*_{(1)})] \,\mathrm{d}\Omega = 0. \tag{27}$$

Due to the relatively high Peclet of this problem, the streamline-upwind Petrov–Galerkin formulation (SUPG) developed by Brooks and Hughes [14] is used to suppress the undesirable oscillations in the calculation of the temperature fields. To solve the equation by this method, an additional weighing function formulation $(\tilde{k}^* \upsilon^*/\upsilon^* \cdot \upsilon^*) \cdot \nabla^* \phi_i$ is applied to all terms of the energy Eq. (16), where $\tilde{k}^*$ used in this paper is defined as:

$$\tilde{k}^* = \left(\tilde{\xi} \upsilon_\xi^* h_\xi^* + \tilde{\chi} \upsilon_\chi^* h_\chi^* + \tilde{\eta} \upsilon_\eta^* h_\eta^* \right)/2 \tag{28}$$

where the definitions of υ_ξ^*, υ_χ^*, υ_η^*, h_ξ^*, h_χ^* and h_η^* are the same as those defined in Eq. (26). Consequently, the following weak forms are finally obtained:

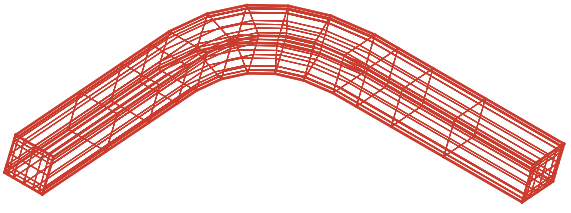

Fig. 2. The finite element mesh used in the current simulation.

$$\int_{\Omega}\{\phi_i[P_e, v^*\cdot\nabla^* T^* - B_r(-p^* \boldsymbol{I} + \boldsymbol{s}^* + 2\eta^* \boldsymbol{d}^*) : \boldsymbol{d}^*] + \nabla^*\phi_i \cdot \nabla^* T^*\}\,\mathrm{d}\Omega - \int_A \phi_i \boldsymbol{n}\cdot\nabla^* T^*\,\mathrm{d}A = 0 \quad (29)$$

where $\phi_i' = \phi_i + (\tilde{k}^* v^*/v^*\cdot v^*)\cdot\nabla^*\phi_i$.

Since the integrals in Eqs. (23)–(25), (27) and (29) are integrals of polynomial functions, they may be readily evaluated numerically using Gaussian quadrature. The above discretization processes lead to a system of non-linear equations of the form

$$K(x^*)x^* = f^* \quad (30)$$

where $\boldsymbol{K}(\boldsymbol{x}^*)$ is global stiffness maxtics, $\boldsymbol{f}^*$ is the force vector; x^* is the unknown variable vector.

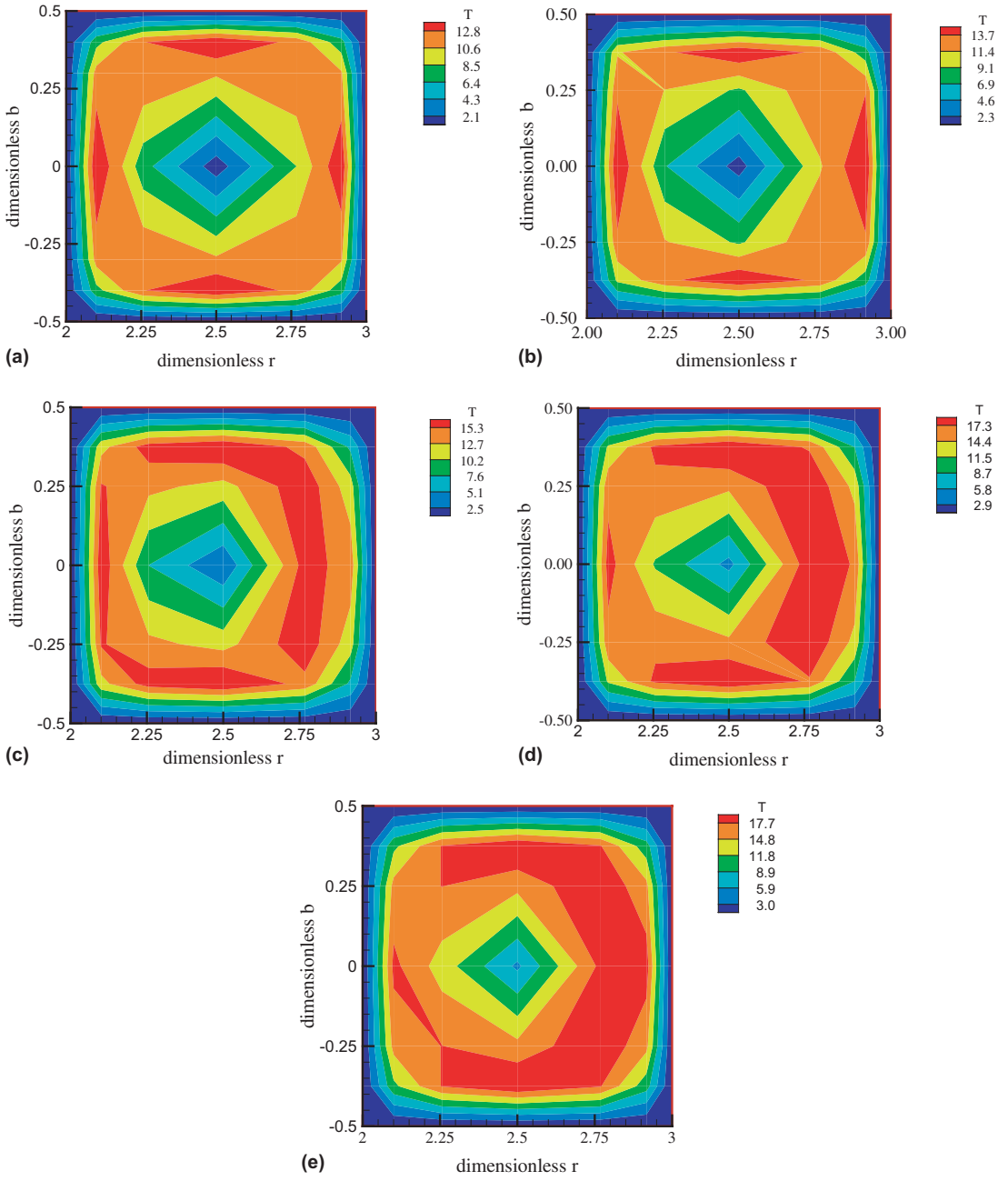

Fig. 3. Dimensionless temperature contours in the cross-section along the streamline for the characteristic shear-rate of $\dot{\gamma}_c = 10$.

The Newton–Raphson iteration method is employed to solve the above set of nonlinear equations. Due to the sparseness and asymmetry of the global stiffness matrix, the biconjugate gradient stabilized (BiCGStab) method [15] has been developed to compute all the unknowns at each iteration step. Convergence is considered to be achieved when the relative error of each of the dimensionless variables is less than 10^{-4}.

4. Results and discussion

The numerical results for the present problem of creeping heat-transfer behavior of a nylon-6 liquid through bent square ducts are presented in this section. The finite-element mesh used for the computation domain is shown in Fig. 2. The local Nusselt number can be defined as the dimensionless temperature gradient [16] at the wall, and the average Nusselt number $\overline{N}_u$ is the Nusselt number averaged over the width of each wall at a specified streamline location. As indicated in Fig. 1, s is the streamline coordinate, r is the coordinate normal to the streamline, and b is the coordinate normal to coordinate s and r. S^*, r^* and b^* are the corresponding dimensionless coordinates defined as:

$$S^* = S/w, \quad b^* = b/w \quad \text{and} \quad r^* = r/w \tag{31}$$

For convenience, we set $S^* = 0$ at the entrance of the curved section of the duct.

The generated thermal field is entirely due to viscous heating. Dimensionless temperature contours in the cross-section along the streamline are plotted in Fig. 3(a)–(e) for the characteristic shear-rate, defined as $\dot{\gamma}_c = U/w$, of $\dot{\gamma}_c = 10$. As the fluid flows through the channel, it is subjected to strong shear in the near-wall region due to the relatively high shear-rate of the flow. As a result, the temperature rises rapidly in this region. The dissipation heat is convected downstream along the channel, with the maximum temperature occurring at the outlet of the channel near the outer wall, due to the high Peclet number and high shear-rate. By contrast, the temperature near the channel center-line region is relatively low. This phenomenon holds for $\dot{\gamma}_c$ ranging from 5 to 20 in this study.

The creeping heat-transfer behavior of this flow problem was studied. Fig. 3 shows the temperature contours in the cross-section along the streamline for the characteristic shear-rate of $\dot{\gamma}_c = 10$. Upstream, the temperature near the outer and inner walls are quite similar. Fig. 3(a) shows this phenomenon at dimensionless streamline locations $S^* = -5$. As the fluid approaches the turn, temperature near the outer wall becomes a little higher than near the inner wall. In the curving section, *the temperature difference between outer and inner walls is found to be significant, as seen in Fig. 3(b) at 15° relative to the start of the turn, in Fig. 3(c) at 60° relative to the start of the turn, and in Fig. 3(d) at the outlet of the turn*. At a small distance after the curve, the temperature along the outer wall is also found to be higher than along the inner wall, as seen in Fig. 3(e) at $S^* = 6.0$.

4.1. Effect of flow-rate

The average Nusselt number $\overline{N}_u$ along the four channel walls are shown in Figs. 4–6 for three flow-rates. Along the outer wall for the curved section, $\overline{N}_u$ is seen to undergo a dip when leaving the turn for all three

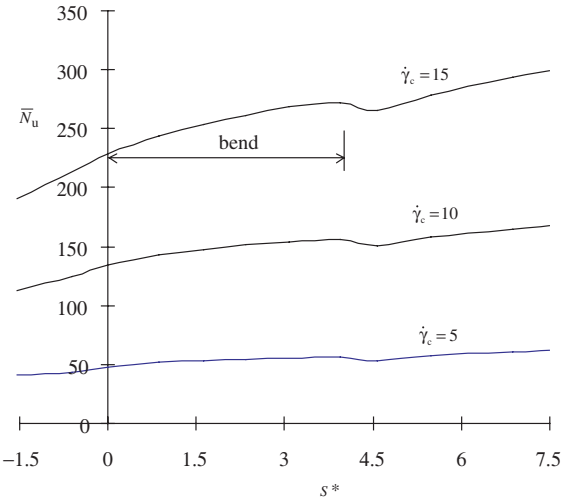

Fig. 4. Effect of flow-rate on the $\overline{N}_u$ distributions along the outer-wall.

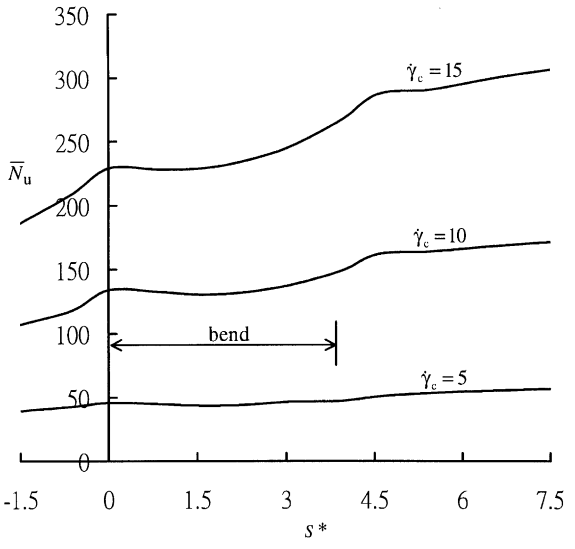

Fig. 5. Effect of flow-rate on the $\overline{N}_u$ distributions along the inner-wall.

flow-rate cases, as seen in Fig. 4. This dip is due to the flow tending to move away from the downstream straight wall, resulting in lower velocity gradient. As seen in Fig. 5 along the inner wall at the beginning of the curved section, $\overline{N}_u$ undergoes a decrease before resuming its increasing trend. This decrease is due to much lower local heat dissipation, which is caused by a lower velocity gradient since the flow tends to move away from the inner curved wall at the entrance. The relative difference of $\overline{N}_u$ between outer and inner walls is plotted in Fig. 7. It is obvious that for low flow-rates, $\overline{N}_u$ is approximately the same for both curved walls. However, as the flow rate increases, the $\overline{N}_u$ along the outer wall becomes significantly higher than that along the inner wall.

In the square-duct geometry of this study for the three flow-rates, $\overline{N}_u$ values along both top and bottom walls are virtually identical, increase with distance along the channel, for all three flow-rates cases, as shown in Fig. 6. The average Nusselt number $\overline{N}_u$ along the four channel walls are shown in Fig. 8 for the case of $\dot{\gamma}_c$ equal to 10. The value of $\overline{N}_u$ along both top and bottom walls

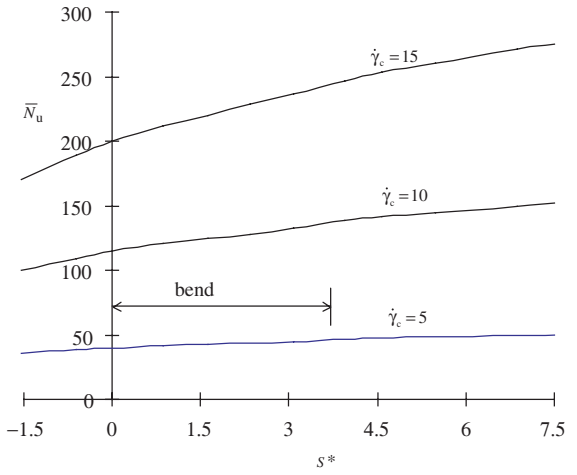

Fig. 6. Effect of flow-rate on the $\overline{N}_u$ distributions along the top and bottom walls.

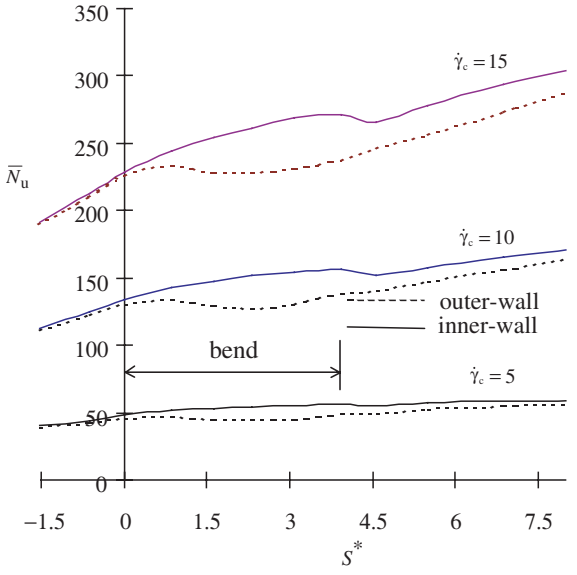

Fig. 7. Comparisons of N_u outer and inner walls for three values of flow-rate.

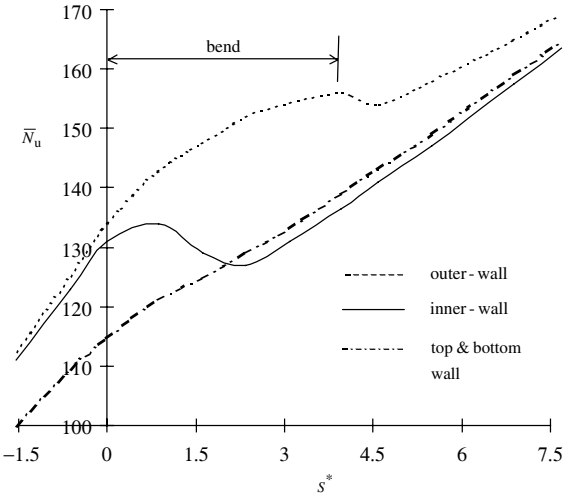

Fig. 8. Effect of flow-rate on the $\overline{N}_u$ distributios along the walls for $\dot{\gamma}_c = 10$.

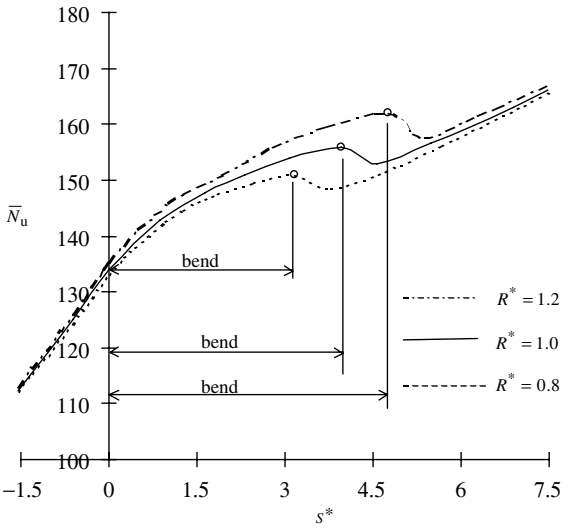

Fig. 9. Effect of corner radius on the $\overline{N}_u$ distributions along the outer-wall.

is smaller than the $\overline{N}_u$ along the outer wall. This phenomenon holds for $\dot{\gamma}_c$ ranging from 5 to 20 in this study.

4.2. Effect of corner radius

In the curved section, $\overline{N}_u$ along the four walls at any *angle* measured relative to the start of the turn are predicted to be greater for larger radii, as shown in Figs. 9–11. The effect of corner radius on $\overline{N}_u$ is only significant in the curved section. For $\overline{N}_u$ along the top and bottom walls illustrated in Fig. 11, it is seen that the effect of corner radius is insignificant.

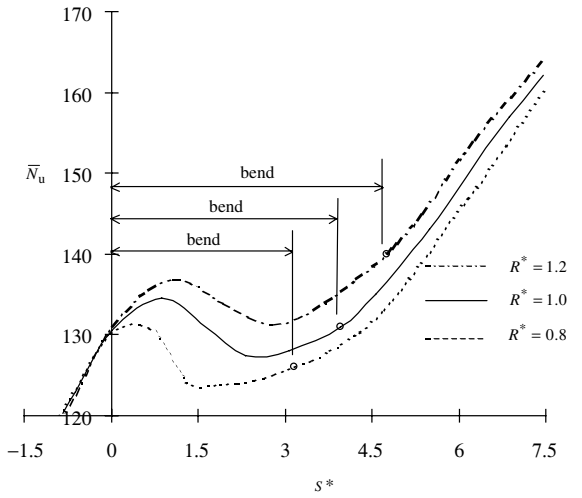

Fig. 10. Effect of corner radius on the $\overline{N}_u$ distributions along the inner-wall.

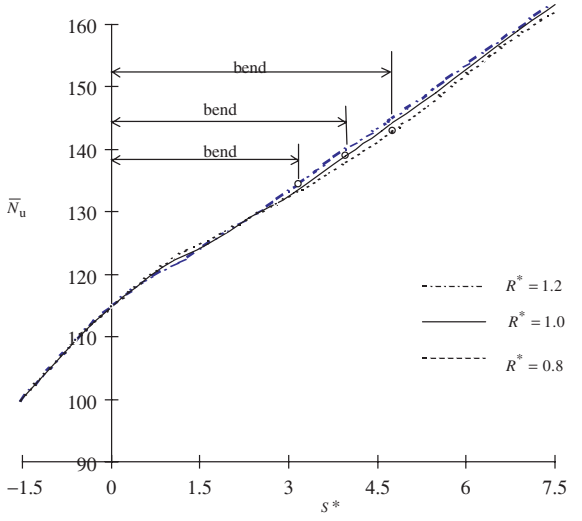

Fig. 11. Effect of corner radius on the $\overline{N}_u$ distributions along the top and bottom walls.

5. Conclusion

A numerical investigation based on EVSS/SUPG finite element method is performed to study the 3D non-isothermal creeping flow of a nylon-6 liquid in square- ducts with uniform temperature. The constitutive equation used is a differential-type non-isothermal White–Metzner model. Since the Dean number is small for this type of flow, centrifugal force is neglected in the momentum equation. The generated thermal field is entirely due to viscous heating.

As the fluid flows through the channel, it is subjected to strong shear in the near-wall region, resulting in rapid temperature rise in this region. The dissipation heat is convected downstream along the channel, with the maximum temperature occurring at the outlet of the channel near the outer wall, due to the high Peclet number and high shear-rate of this flow. By contrast, the temperature near the channel center-line region is relatively low.

Along the outer wall of the curved section, $\overline{N}_u$ is seen to undergo a dip when leaving the turn. $\overline{N}_u$ along the inner wall undergoes a decrease before resuming its increasing trend when fluid enters the curved section. For the square-duct geometry of this study, the value of $\overline{N}_u$ for both top and bottom walls is virtually identical, and is smaller than the $\overline{N}_u$ along the outer walls.

The effects of flow-rate, and channel geometry on the average Nusselt number along the duct walls. The effect of increasing flow-rate is seen to increase Nusselt number. $\overline{N}_u$ is approximately the same for both curved walls for low flow-rates. However, for high flow-rates, the $\overline{N}_u$ along the outer wall becomes significantly higher than that along the inner wall. The effect of corner radius on $\overline{N}_u$ is only significant in the curved section. Far downstream of the channel, these thermal properties are little affected by the corner radius.

References

[1] S.T. Hwang, S.W. Hong, Forced convection heat transfer in square ducts, Chem. Eng. Prog. Symp. Ser. 66 (1970) 100–108.

[2] M.T. Ahmadian, L.C. Burmeister, R.W. Johnson, Three-dimensional solidification and flow of polymers in curved square ducts, Polym. Eng. Sci. 29 (2) (1989) 91–99.

[3] D.R. Oliver, S.S. Rao, Heat transfer to pseudolastic fluids in laminar flow in horizontal tubes, Trans. Inst. Chem. Engrs. 56 (1978) 62–66.

[4] B. Mena, G. Best, T. Sanchez, Heat transfer in non-Newtonian flow through pipes, Rheol. Acta 17 (1978) 455–477.

[5] J.P. Hartnett, M. Kostic, Heat transfer to Newtonian and non-Newtonian fluids in rectangular ducts, Adv. Heat Transfer 19 (1989) 247–256.

[6] C. Xie, J.P. Hartnett, Laminar heat transfer of Newtonian and non-Newtonian fluids in a 2:1 rectangular duct, Int. J. Heat Mass Transfer 35 (1992) 641–648.
[7] W.R. Dean, Note on the motion of fluid in a curved pipes, Proc. Roy. Soc. London 121 (1928) 402–420.
[8] B.A. Finlayson, Numerical Methods in Heat Transfer, Wiley, New York, 1985, pp. 150–156.
[9] J.M. Marchal, M.J. Crochet, A new mixed finite element for calculating viscoelastic flow, J. Non-Newtonian Fluid Mech. 26 (1987) 77–114.
[10] M.A. Mendelson, P.W. Yeh, R.A. Brown, Finite element calculation of viscoelastic flow in a journal bearing: I. Small eccentricities, J. Non-Newtonian Fluid Mech. 10 (1982) 31–62.
[11] F. Debae, V. Legat, M.J. Crochet, Practical evaluation for mixed finite element methods for viscoelastic flow, J. Rheol. 38 (2) (1994) 421–443.
[12] G.H. Wu, S.J. Ju, Numerical prediction of non-isothermal folw of NYLON-6 past a cylinder between plates, J. Polym. Eng. 19 (4) (1999) 287–304.
[13] M. Lawal, D.M. Kalyon, Numerical solution for combined free and forced convection in horizontal parallel plates with asymmetrical heating, Num. Heat Transfer 26 (1994) 103–121.
[14] A.N. Brooks, T.J. Hughes, Steamline upwind/Petrov–Galerkin formulation for convection dominated flows with particular emphasis on the incompressible Navier–Stokes equations", Comp. Meth. Appl. Mech. Eng. 32 (1982) 199–259.
[15] H.A. Van Der Vorst, BiCGSTAB: a fast and smoothly converging variant of Bi-CG for the solution of nonsymmetric linear system, SIAM J. Sci. Atat. Comput. 13 (1992) 631–653.
[16] F. Kreith, S. Bohn, Priciple of Heat Transfer, West Publishing, Singapore, 1993, pp. 250–254.